Power-law fluctuations near critical point in semiconductor lasers with delayed feedback

Tomoaki Niiyama[1,*] and Satoshi Sunada[1,2]

[1]*Institute of Science and Engineering, Kanazawa University, Kakuma-machi, Kanazawa, Ishikawa 920-1192, Japan*

[2]*Japan Science and Technology Agency (JST), PRESTO, 4-1-8 Honcho, Kawaguchi, Saitama 332-0012, Japan*

(Received 7 December 2021; revised 8 September 2022; accepted 2 December 2022; published 22 December 2022)

Since the analogy between laser oscillation and second-order phase transition was indicated in the 1970s, dynamical fluctuations on lasing threshold inherent in critical phenomena have gained significant interest. Here, we numerically and experimentally demonstrate that a semiconductor laser subject to delayed optical feedback can exhibit unusual large intensity fluctuations characterized by power-law distributions. Such an intensity fluctuation consists of distinct intermittent bursts of light intensity, whose peak values attain tens of times the intensity of the maximum gain mode. This burst behavior emerges when a laser with a long time delay (over 100 ns) and an optimal feedback strength operates around the lasing threshold. The intensity and waiting time statistics follow power-law-like distributions. We also report on the experimental results that suggested power-law intensity dynamics in a semiconductor laser with delayed feedback. The reason for the emergence of power-law behavior in the laser system is discussed from the perspective of nonequilibrium-critical behavior in a slowly driven-dissipative system known as self-organized criticality.

DOI: 10.1103/PhysRevResearch.4.043205

I. INTRODUCTION

Laser oscillation has gained interest in the areas of theoretical physics as well as engineering application since the analogy between laser oscillation and second-order phase transition was indicated by DeGiorgio and Scully [1] and Graham and Haken [2]. The analogy to the second-order phase transition has inspired significant interest not just in the transition of a macroscopic quantity, i.e., the onset of laser oscillation, but also its fluctuation around the lasing threshold, which is regarded as a critical point [3–7]. However, despite many studies on this fluctuation of light intensity, scale-invariant fluctuations expected from the context of equilibrium critical phenomena have not been reported.

The scale-invariant feature mentioned here implies that variable s such as magnitude, duration, or waiting time of an energy-releasing event follows a *power-law distribution*,

$$P(s) \propto s^{-\beta}, \tag{1}$$

where β denotes the characteristic exponent. Power-law distributions, which are generalized as Lévy's stable distributions, have a scale-invariant feature because their mean, variance, and higher order of moments cannot be determined mathematically under a certain condition of the exponent and the upper bound of s [8]. Thus, dissipation phenomena characterized by the statistical distribution provide substantially large fluctuation and intermittency in their energy dissipation. Such a statistical feature can be found in various natural phenomena and physical systems, e.g., solar flares [9], earthquakes [10,11], plasticity [12,13], sandpiles [14,15], magnetization [16], and superconductors [17,18].

This scale-invariant feature can be observed in equilibrium-critical phenomena: for instance, the area of the magnetized domain in the Ising model. Laser systems differ from those that exhibit equilibrium-critical phenomena in many aspects such that laser is a kind of nonequilibrium systems. One of the most significant differences is the degrees of freedom of the system. Laser dynamics consists of only a few dynamical variables, such as the electric field and carrier density [19], whereas equilibrium-critical systems have many degrees of freedom. However, it is well known that delayed feedbacks provide high dimensionality to the laser dynamics [19–23]. Generally, delay systems can be represented as spatially expanded systems, where numerous independent elements, the so-called virtual nodes that correspond to many degrees of freedom, interact with themselves in a time domain. Hence, delayed feedback can provide multiplicity of the processes and their interactions to the system through high dimensionality.

In addition to the high dimensionality, the delayed feedback also provides a wide variety of dynamical behaviors with laser systems [19,23,24]. For instance, external light injection with a time delay can cause regular sequential pulsation in a short timescale, the so-called rapid pulse packages (RPPs) [25], and irregular behaviors, known as optical turbulence, under a strong optical feedback condition [26]. Low pump-current conditions near the lasing threshold yield a complex fluctuation, called low-frequency fluctuations (LFF), consisting of subnanosecond intensity pulses and regular intensity drops with a longer timescale [24,27,28]. Temporal fluctua-

*niyama@se.kanazawa-u.ac.jp

tions of intermittent pulsation in similar low pumping-power conditions have been investigated and analyzed in terms of intermittent dynamics and extreme events [29–33]. In addition, the existence of virtual nodes and their interplay have been used for delay-based computing [34,35].

This high dimensionality and complexity originating from delayed feedback may provide a laser system scale-invariant fluctuations near the lasing threshold. In this paper, we show the statistical distributions and their features in the intensity dynamics of semiconductor lasers with delayed feedback by conducting numerical simulations and supplementary experiments. In Sec. II, we demonstrate through numerical simulations of the Lang–Kobayashi model that a semiconductor laser with long and strong delayed feedback exhibits intermittent intensity bursts characterized by power-law distributions. Then, the condition to obtain a remarkable power-law feature is elucidated based on the simulation results. In Sec. III, we report the experimental results, which partly support the numerical results. Finally, in Sec. IV, we discuss the emergence of the power-law behavior for the proposed laser system from the viewpoint of the conditions to achieve criticality in slowly driven-dissipative systems.

II. NUMERICAL SIMULATION

A. Numerical simulation setup

In the present paper, we employ the Lang–Kobayashi model represented by the complex electric field $\hat{E}(t)$ and carrier density $N(t)$ at time t for the simulation of a semiconductor laser with a single delayed feedback [19,36],

$$\frac{d\hat{E}}{dt} = \frac{1+i\alpha}{2}\left[G_N\{N(t)-N_0\} - \frac{1}{\tau_p}\right] \times \hat{E}(t) + \kappa \hat{E}(t-\tau)e^{-i\omega_0\tau}, \tag{2}$$

$$\frac{dN}{dt} = J - \frac{N(t)}{\tau_s} - G_0\{N(t)-N_0\}|\hat{E}(t)|^2, \tag{3}$$

$$G_N = \frac{G_0}{1+\epsilon|\hat{E}(t)|^2}, \tag{4}$$

where α, G_0, N_0, τ_p, τ_s, ω_0, and ϵ are the linewidth enhancement factor, gain coefficient, carrier density at transparency, photon lifetime, carrier lifetime, optical angular frequency, and gain saturation parameter, respectively. Here, J, κ, and τ represent the pump current, feedback strength, and external round-trip time corresponding to the delay time, respectively. We used the following set of parameters for the simulations: $\alpha = 5, t_p = 1.927 \times 10^{-12}\,\mathrm{s}, t_s = 2.04 \times 10^{-09}\,\mathrm{s}, N_0 = 1.4 \times 10^{+24}\,1/m^3$, $\omega_0 = 1.226 \times 10^{+15}\,\mathrm{s}^{-1}$, and $G_0 = 1 \times 10^{-12}\,\mathrm{m}^3/s$. The gain saturation parameter is set as zero except for the simulations in Appendix B. The fourth-order Runge–Kutta method was used to numerically integrate the Lang–Kobayashi model. The timestep for the integration was set to 1 femtosecond.

A normalized pump current defined as $j = J/J_{th}$ is used in the simulations, where J_{th} is the threshold value of the solitary oscillation mode, $J_{th} = N_{th}/\tau_s$, and $N_{th} = N_0 + 1/(\tau_p G_0)$. Notably, the laser can oscillate below the threshold current $j = 1$ because some external cavity modes that originate from the delayed feedback have lower thresholds than the threshold

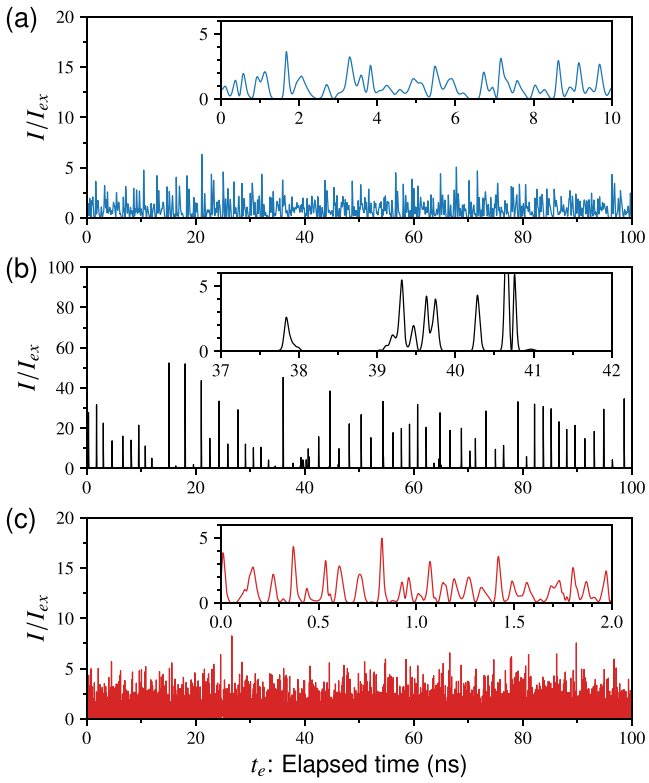

FIG. 1. Time series of normalized laser intensity obtained from the numerical simulations under the condition of $\tau = 1\,\mu$s and $\kappa = 60\,\mathrm{ns}^{-1}$, where the horizontal axis represents the elapsed time from 1999.5 μs. The normalized pump currents are (a) $j = 0.9579$, (b) $j = 1$, and (c) $j = 3.5589$. Irregular and intermittent pulsation (intensity bursts) with high intensity is observed at the threshold pump current, $j = 1$.

of the solitary mode. We also normalize the laser intensity, $I = |\hat{E}|^2$, by that of the maximum gain mode,

$$I_{ex} = \frac{1}{G_N}\frac{\tau_p}{\tau_s}\frac{(j-1)N_{th}G_N + 2\kappa}{1-2\tau_p\kappa}, \tag{5}$$

where the maximum gain mode is the most efficient oscillation mode, with the lowest lasing threshold, among the external-cavity modes [19]. The derivation of the equation is described in Appendix A.

As initial conditions of the electric field and carrier density, those of the maximum gain mode were applied, $\mathrm{Re}[\hat{E}(0)] = \mathrm{Im}[\hat{E}(0)] = \sqrt{I_{ex}}$, $N(0) = N_{ex}$, where $N_{ex} = N_{th} - (2\kappa/G_N)$. For the initial condition of the delayed electric field $[\hat{E}(t)$ for $-\tau \leqslant t < 0]$, a random electric field, $\hat{E}(0)$ with 1% random noise generated by uniform random numbers, was used. We confirmed that the initial condition does not affect the dynamical behaviors as long as a sufficiently long simulation time is taken.

B. Temporal behavior

Figure 1 shows the time series of normalized intensity $I(t)/I_{ex}$ obtained from the simulation with a long delay time $\tau = 1\,\mu$s, strong optical feedback $\kappa = 60\,\mathrm{ns}^{-1}$, and different pump currents ($j = 0.9579$, 1, and 3.5589). The time series is

shown as a function of the elapsed time from $t = 1999.5\,\mu s$. As shown in Fig. 1(b), a distinct behavior appears on the condition that the pump current is just the threshold current, i.e., $j = 1$; irregular sharp pulses (intensity bursts) originate abruptly from a state of almost zero intensity. On the contrary, as shown in Figs. 1(a) and 1(c), only chaotic fluctuation around a mean intensity, $I/I_{ex} \simeq 1$, is observed when the currents that deviate from the threshold value are applied ($j = 0.9579$ and 3.5589). It should be noted that the intensity rarely takes on a value near zero when $j = 0.9579$ and 3.5589. This is in contrast to the case of $j = 1$. Here, we note that a sufficiently long simulation time is required to observe such intensity bursts shown in Fig. 1(b) because of the presence of a long transient regime in the early stage with quiescent intervals and quasiperiodic pulses.

Another significant feature is its scale-free burst-like pulsation behavior. The peak heights of certain bursts attain several tens of times the steady intensity of the maximum gain mode I_{ex}. Recalling that I_{ex} means the highest possible intensity produced by steady-state oscillation, we can consider that the threshold condition provides a highly efficient laser oscillation. On the other hand, significantly small bursts occur as observed in the insert in Fig. 1(b). Although not apparent in the figure, there are many tiny pulses that are significantly smaller than I_{ex}. As an example, one can find out a tiny pulse at 40.9 ns in the inset figure.

C. Statistical distribution

To demonstrate the existence of scale-invariant fluctuations characterized by power-law distributions in the laser oscillations, we here present statistical distributions of the laser intensity and intervals of the bursts calculated from the time series of the numerical simulations.

The probability density functions (PDFs) of the normalized intensity I/I_{ex} are shown in Fig. 2, where the probability distributions are depicted in a double logarithmic display. Under the threshold condition ($j = 1$), the distribution evidently forms a straight shape (open-black circles), i.e., the distribution contains a power-law decay described by Eq. (1), over at least three orders of magnitude, where the characteristic exponent is almost unity ($\beta \simeq 1$). The exponent is close to that observed in seismic statistics known as Gutenberg–Richter's law [37]. When $j > 1$, the power-law decay (scale-invariant feature) disappears rapidly and transforms to an exponential one, which has a characteristic scale. When $j < 1$, the power-law feature also disappears, as can be seen from the distribution represented by blue diamonds in Fig. 2. It should be noted that the cutoff intensity of the distributions, i.e., the upper bound of the event size, takes on a maximum value under the threshold condition $j = 1$. We will investigate this trend in detail in Sec. II E.

It is known that critical behavior in nonequilibrium systems yields power-law statistics in terms of size and the time of energy-release events [9,14,18]. Here, the distributions of waiting time, i.e., the time interval between two sequential peaks of intensity bursts, are shown in Fig. 3, where we consider each burst of intensity as an energy-release event. The waiting time distribution obtained for a large pump current ($j = 3.5589$) forms a convex shape around $t_w = 0.04$ ns.

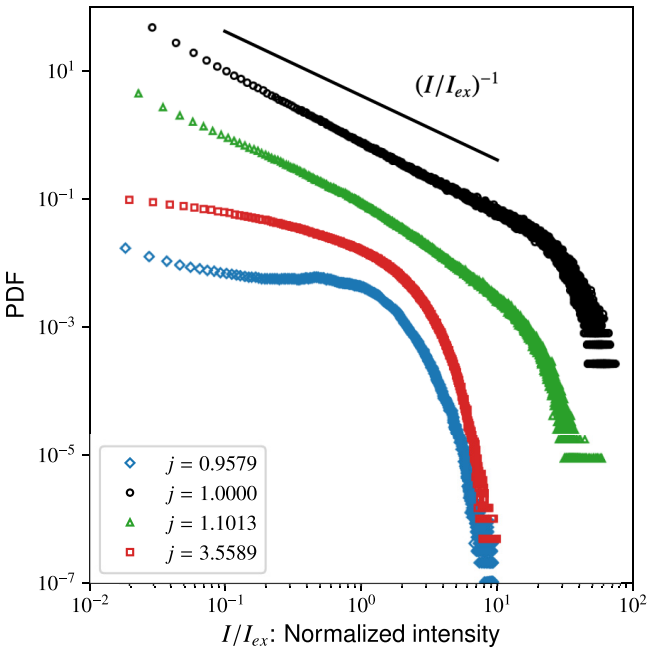

FIG. 2. Probability density function (PDF) of the normalized intensity I/I_{ex} obtained from the numerical simulations, where the PDFs are shifted arbitrarily in the vertical direction for visibility. The distribution of the probability density of $j = 1$ (black circles) clearly exhibits an algebraic decay with exponent $\beta \simeq 1$, where the solid straight line represents $(I/I_{ex})^{-1}$. The cutoff of the distributions is maximized at $j = 1$.

This means the existence of a characteristic timescale of the burst events. With decreasing the pump current from the large value, a straight "shoulder," which is an indication of a power-law character, develops in the distributions. Under the threshold condition ($j = 1$), a power-law decay with $\beta \simeq 3/2$ clearly appears over approximately two orders of magnitude

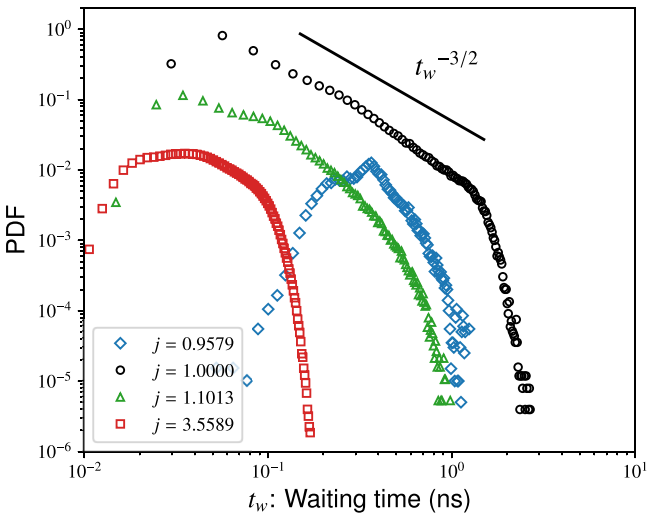

FIG. 3. PDF of waiting time, the interval between successive peaks of intensity bursts, obtained with an injection current j. The power-law regime appears when $j = 1$ (black circles), where the solid line represents a power-law curve with $\beta = 1.5$.

as depicted by open black circles in Fig. 3. This power-law feature in the waiting time is compatible with the aftershock statistics of earthquakes known as Utsu–Omori's law, while the exponent of 3/2 is slightly higher than that of the law [10,11]. Similar to the case with the intensity statistics shown in Fig. 2, the power-law behavior disappears again for lower pump currents ($j < 1$), which are depicted by blue diamonds in Fig. 3.

The above simulation results show that the statistical distributions of size and interval of energy-release events form power-law decays just on the threshold condition $j = 1$. This indicates that semiconductor lasers with optical feedback exhibit power-law statistics in the threshold condition of the solitary mode.

D. Trajectory

In this subsection, we observe the intensity dynamics exhibiting power-law fluctuations as a trajectory in the phase space of time-delayed dynamical systems. In the Lang-Kobayashi model, a space consisting of the phase difference $\Phi(t) = \phi(t-\tau) - \phi(t)$ and carrier density $N(t)$ is called the "phase space" of the system. This space is only a projection of the rigorous phase-space. However, it is commonly used to observe complex delay dynamics such as LFFs and RPPs [19,25,27], because this phase space allows us to visually understand the relationship between a trajectory and stationary points. We here observe the phase space consisting of the laser intensity $I(t)/I_{ex}$ rather than $N(t)$ since we have focused on the large intensity fluctuation in this paper.

A part of a trajectory calculated from the numerical result accompanying the power-law behavior is shown in Fig. 4. Here, the simulation condition is identical to that used in Figs. 1(b) and 2, $\tau = 1\,\mu$s, $\kappa = 60\,\text{ns}^{-1}$, and $j = 1$. The curve in the figure represents the trajectory following 1999.5 μs. The blue solid circles are the stationary points of external cavity modes. The figure shows certain unusual motions of the trajectory: the trajectory moves largely omitting many stationary points when $\Phi(t)$ decreases and increases abruptly in the direction of increasing $\Phi(t)$ (occasionally with a jerking motion).

The remarkably sticky motion of the trajectory is noteworthy: The trajectory sometimes orbits several narrow regions although there are no stationary points in the regions. Some typical regions are indicated by white arrows in Fig. 4(b). The narrow areas where the trajectory winds and/or slows down can be regarded as points; hence, we refer to these points as "pseudo-" stationary points. The dynamics is more significantly affected by the pseudo-stationary points than the "ordinary-" stationary points depicted by the blue circles in the figure. In LFFs and RPPs, trajectories follow a sequence from one ordinary-stationary point to the next, heading toward the maximum gain mode and returning to the minimum gain state after reaching the mode [19,25,27]. In contrast, the trajectory of the present power-law dynamics is trapped by various pseudo-stationary points as well as the ordinary-stationary points and irregular jumps along the phase difference (in the horizontal direction). This is an obvious difference between the present dynamics and traditional complex dynamics, such as LFFs or RPPs.

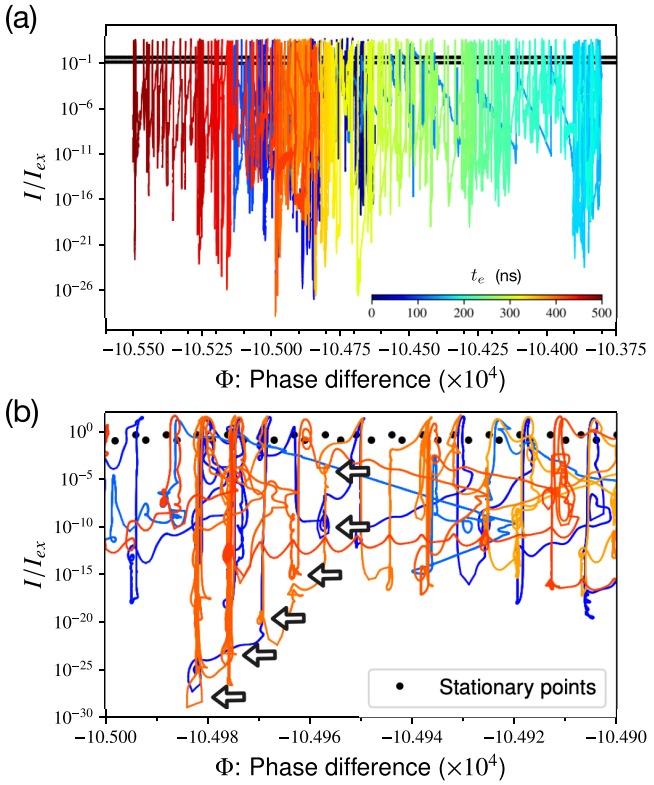

FIG. 4. A trajectory in the phase space constructed by phase difference Φ and normalized intensity I/I_{ex} in the condition that $\tau = 1\,\mu$s, $\kappa = 60\,\text{ns}^{-1}$, and $j = 1$, where the solid blue circles are stationary solutions of the Lang–Kobayashi equation. (a) The trajectory is depicted by color according to the elapsed time, t_e, from $t = 1999.5\,\mu$s. (b) Enlarged figure from $\Phi = -10.500$ to -10.490. The white arrows indicate typical pseudostationary points (see text).

Further, the pseudo-stationary points seem to be (logarithmically) homogeneously distributed in a region that extends from extremely small to large intensities in the phase space. Thus, the power-law fluctuation is expected to extend to a significantly smaller region of intensity than that depicted in Fig. 2. The appearance of such multiscale pseudo stationary points may be related to the power-law behavior in the intensity dynamics. A more detailed analysis of the phase space dynamics would be reported elsewhere.

E. Condition for power-law behavior

In this subsection, evaluating the extent of the power-law behaviors systematically in various conditions of delay time τ and feedback strength κ, we reveal the condition of the emergence of the power-law behaviors illustrated in the previous subsection. To achieve this, we calculate the mean value of the *exceedance* of intensity, $\langle I \rangle|_{>a}$, i.e., the size of the events beyond a reference value a [8], from the simulation results. As shown in Fig. 2, the distribution exhibits an evident power-law decay as the cutoff of the distribution increases toward the rightmost part of the figure. Thus, the mean exceedance normalized by the maximum gain mode intensity $\langle I \rangle|_{>I_{ex}}/I_{ex}$ can be a good indicator of the manifestation of power-law behaviors [8], where we use I_{ex} as the reference value for the

exceedance calculation. To represent the dependence of the pump current, we employ another normalized pump current defined by

$$j_e \equiv \frac{J - J_{ex}}{J_{th} - J_{ex}} = (j-1)\frac{N_{th}G_N}{2\kappa} + 1, \tag{6}$$

where J_{ex} is the threshold pump current of the maximum gain mode defined by $J_{ex} = J_{th}[1 - 2\kappa/(N_{th}G_N)]$ (see Appendix A). Thus, $j_e = 0$ and $j_e = 1$ correspond to the threshold currents of the maximum gain mode and solitary mode, respectively.

The dependence of the normalized mean exceedance $\langle I\rangle|_{>I_{ex}}/I_{ex}$ on the delay time τ is shown as a function of the pump current in Fig. 5(a). Here, we employed the time series after $t = 1900\,\mu$s to calculate the mean exceedance. The figure shows a remarkable feature that $\langle I\rangle|_{>I_{ex}}/I_{ex}$ forms a sharp peak around the threshold current of the solitary mode $j_e = 1$, when the delay time is sufficiently long ($\tau > 1$ ns). This peak clearly represents the manifestation of the power-law behavior at the threshold of the solitary mode. The exceedance $\langle I\rangle|_{>I_{ex}}/I_{ex}$ approaches unity as j_e increases from the threshold current. This indicates that the excess pump current changes the power-law behavior accompanying extreme intensity bursts to steady oscillation with relatively small fluctuations. On the other hand, $\langle I\rangle|_{>I_{ex}}/I_{ex}$ monotonically decreases as $j_e \to 0$ despite the divergence of $1/I_{ex}$ at $j_e = 0$. This intensity disappearance implies that the maximum gain mode no longer works at the threshold condition of the mode.

As shown in Fig. 5(b), similar peaks indicating the emergence of the power-law behavior and the decay trend can be observed around $j_e = 1$, but it is noteworthy that the peak disappears under an excessively large (or small) feedback strength condition. This result implies the presence of a suitable feedback strength for the power-law behavior. To identify the suitable condition, we depict the relationship between $\langle I\rangle|_{>I_{ex}}/I_{ex}$ with $j_e = 1$ and the normalized feedback strength κ/κ_{max} in Fig. 5(c), where $\kappa_{max} = 1/(2\tau_p) \simeq 260\,\text{ns}^{-1}$ which is the maximum value of the feedback strength as long as I_{ex} is finite [see Eqs. (5) and (A5)]. In the figure, the standard deviation depicted by open black triangles as well as $\langle I\rangle|_{>I_{ex}}/I_{ex}$ has a maximum value at $\kappa/\kappa_{max} \simeq 0.6$.

The results presented in this subsection reveal an emergence condition of the power-law feature: The laser oscillation with the power-law statistics emerges under the condition that the pump current is just on the threshold value of the solitary mode and the delay time is sufficiently long ($\tau > 1$ ns). In addition, the power-law behavior is most remarkable when the feedback strength is approximately 60% of the upper limit.

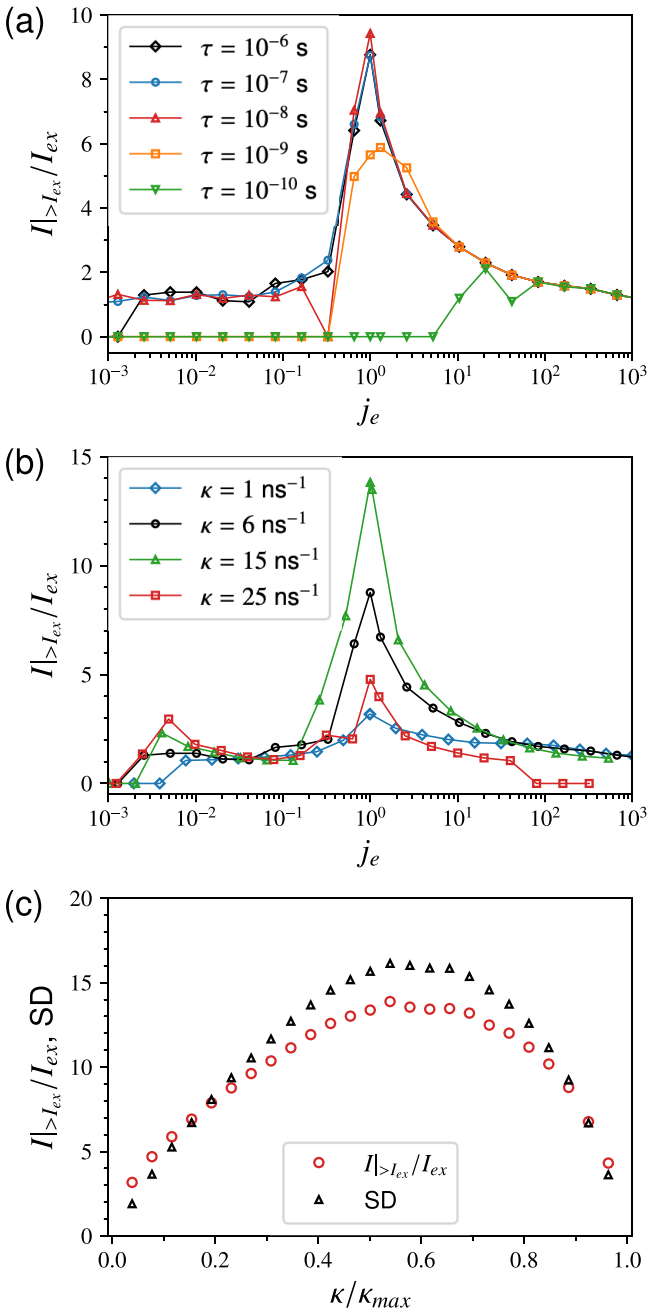

FIG. 5. Mean exceedance of the intensity $\langle I\rangle|_{>I_{ex}}$ as a function of the normalized pump current j_e or feedback strength κ/κ_{max}, where $\langle I\rangle|_{>I_{ex}}$ is normalized by I_{ex}. The mean values are obtained under the condition of (a) various delay times τ and a common feedback strength $\kappa = 60\,\text{ns}^{-1}$, (b) different κ and a common delay time $\tau = 1\,\mu$s, or (c) $\tau = 1\,\mu$s and $j_e = 1$, where the black triangles represent the standard deviation of $\langle I\rangle|_{>I_{ex}}/I_{ex}$.

III. EXPERIMENTAL OBSERVATION

In the previous section, we have demonstrated the power-law behavior of laser intensity in the vicinity of the solitary mode with long time delay and strong feedback by performing numerical simulations. Here, we report the experimental results that support the power-law behavior of the burst intensity dynamics presented in the previous section.

A. Experimental setup

Figure 6 shows the experimental setup to measure the intensity time series of a semiconductor laser with delayed feedback. We used a distributed feedback (DFB) laser (operating at 1550 nm) with a fiber feedback loop. The laser light is split into two portions by a 50/50 fiber coupler. One is sent to the photodetector (Bandwidth 12 GHz) via an optical isolator,

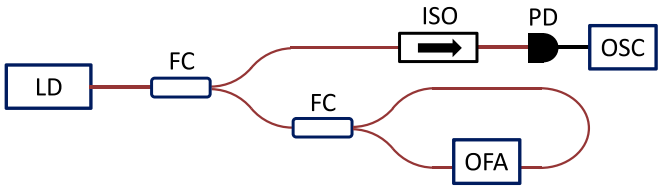

FIG. 6. Experimental setup for a semiconductor laser with delayed feedback. LD, distributed feedback (DFB) laser diode; FC, 50/50 fiber coupler; ISO, optical isolator; PD, photodetector; OSC, oscilloscope; OFA, optical fiber amplifier. The fiber loop is composed of polarization-maintaining fibers.

and the intensity signal is measured with a digital oscilloscope (Bandwidth 16 GHz, 100 GSamples/s). The other is sent to an optical fiber amplifier and fed back to the DFB laser again. In this experiment, the laser current was fixed at 12.04 mA (∼1.2 times of the threshold current) to measure the laser intensity signal clearly. The delay time was set as approximately 116 ns, which is sufficiently long to induce the power-law like behavior. We used the optical fiber amplifier to achieve a strong optical feedback, and controlled the feedback ratio (represented by R) between the feedback power and output power from the laser to be within the range from 0 % to 22 %.

It should be noted that the power-law behavior is difficult to measure in the present experiment because of the limitation of the dynamic range of the measurement, i.e., the limitation of the measurement range of the 8 bit analog-digital converter in the oscilloscope. Thus, the present experiment focus on the appearance of the intermittent burst of the intensity pulses, which is a signature of the power-law behavior reported in the previous section.

B. Temporal behavior

Figure 7 shows typical examples of intensity time series of laser oscillation obtained from our experiments at $J =$ 12.04 mA. The time series at a low feedback-power ratio of $R = 6.6$ % does not indicate a significant burst [Fig. 7(a)]. On the other hand, irregular intensity bursts emerge when R increases [Fig. 7(b)] and become inactive for a large feedback ratio of $R = 22.5$ %, where the intensity fluctuates around a mean value. This dependence on feedback strength is consistent with our simulation results depicted in Figs. 5(b) and 5(c).

C. Statistical distribution

Probability density functions of the intensity obtained from the experimental time series at certain typical conditions are shown in Fig. 8(a), where the time series until 40 μs is used for the calculation. In the figure, the distributions are shifted arbitrarily in the vertical direction for visibility.

A sufficient pump current for laser oscillation without delayed feedback ($J = 12.04$ mA, $R = 0$ %) yields only a Gaussian-like distribution, which is depicted as green circles in the figure. This reflects the fluctuation behavior near the mean intensity. When the optical feedback is applied, the fluctuation is increased dramatically, and the regime of power-law-like decay appears in the statistical distribution. As shown by the black triangles in Fig. 8(a), the power-law regime is

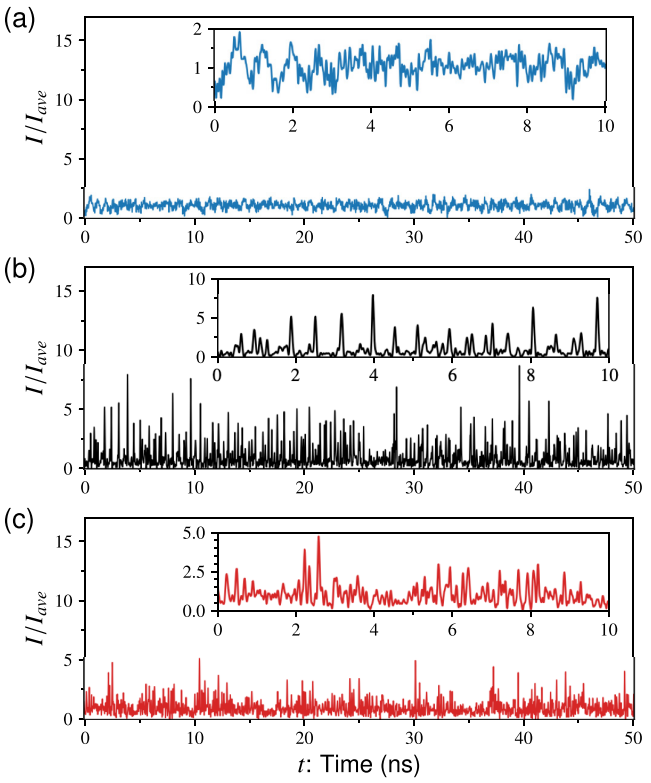

FIG. 7. Time series of light intensity at (a) $R = 6.6$%, (b) 13%, and (c) 22.5%. Enlarged time series are presented in each figure.

indicated by the dashed line in the figure, and the characteristic exponent is approximately two ($\beta \simeq 2$). This experimental condition ($J = 12.04$ mA, $R = 13$ %) is identical to that of Fig. 7(b).

As our numerical simulations predict that this power-law behavior disappears when the feedback strength is significantly larger, the same tendency can be observed in the present experiments. Figure 8(b) shows statistical distributions of relative intensity under the fixed pump current ($J =$ 12.04 mA) and different feedback strengths ($R = 6.6$, 9.7, 13, and 22.5 %), where the intensity is normalized by the mean intensity $I_{\rm ave}$. The figure reveals that the power-law regime becomes prominent in the distribution when the feedback strength increases, but becomes less prominent when the strength exceeds 13 %. The cutoff of the distributions, i.e., the maximum relative intensity, also has a character similar to that of the numerical results as shown in Fig. 2: the cutoff becomes maximum at $R = 13$ % even the difference among the cutoffs is also not clear.

IV. DISCUSSION

This paper shows that intermittent intensity bursts characterized by power-law statistics emerge and are prominent when the delayed feedback is sufficiently long and strong and the pump current is just on the lasing threshold. In order to explain the power-law behavior, as a starting point for the discussion, it would be natural to focus on the nonequilibrium-critical phenomena in slow driven-dissipative systems known as self-organized criticality (SOC), a

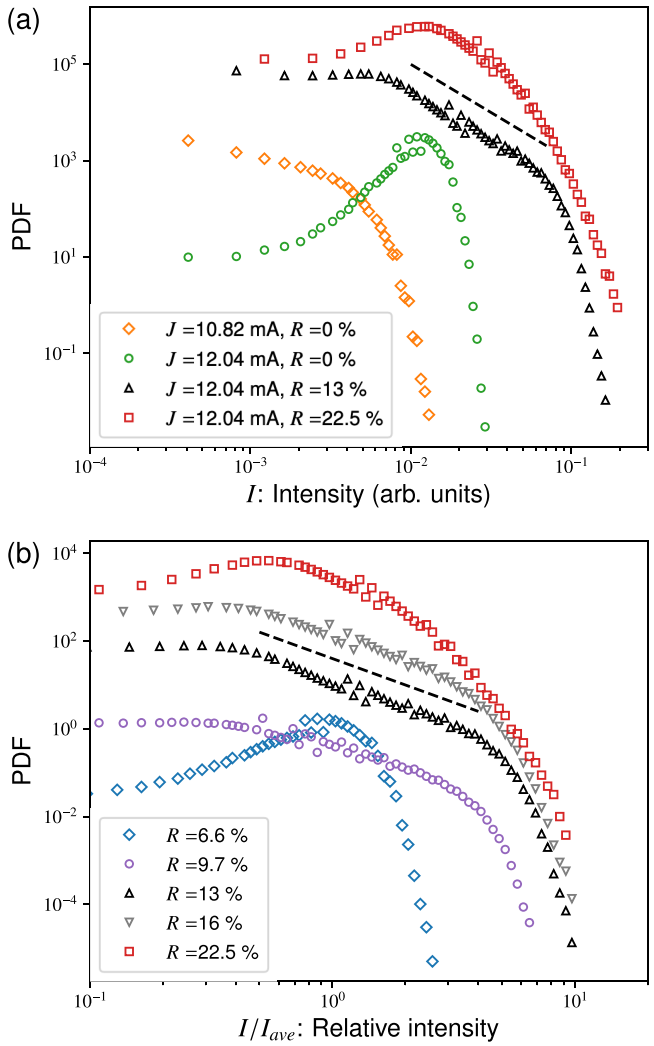

FIG. 8. Experimentally obtained PDF of intensity. Here, all the plots are shifted arbitrarily in the vertical direction for visibility. (a) Intensity distributions obtained under the condition. The distribution of $J = 10.82$ mA and $R = 0$ % is shown by orange diamonds, where the laser oscillates did not occur. The others are the distributions with $J = 12.04$ mA and different feedback strengths R. (b) Intensity distribution normalized by the mean intensity I_{ave}. All the pump currents are set as $J = 12.04$ mA. The dashed lines represent the power-law curve with the exponent $\beta = 2$.

mechanism that produces similar power-law distributions [14,15]. SOC is a phenomenon that a dissipative system spontaneously organizes itself to a critical state that is characterized by scale-invariant statistics, i.e., power-law distribution. It is considered that the emergence of the criticality requires several conditions for a system that stores the energy injected by external driving [18]: (i) the system dissipates the stored energy through *multiple* energy-release processes. (ii) the processes interact with each other, and (iii) the processes have threshold values for activation, and (iv) the rate of energy injection into the system is sufficiently slower than that of the energy-release processes.

The external energy injection of the laser system considered in this paper is the pump current j. In laser systems without feedback, the slowest driving rate corresponds to the threshold current ($j = 1$) rather than zero pump current ($j = 0$). This is because the carrier density of the laser decays with lifetime τ_s even in the absence of energy release by laser oscillation [see Eq. (3)]. Thus, the threshold current can be regarded as the ideal situation that satisfies the fourth condition. The number of virtual nodes of a time-delay dynamical system is proportional to the delay time τ [19]. Furthermore, the strength of the interaction between the feedback and laser intensity is determined by the coupling strength of the feedback, κ. Hence, a sufficiently long τ is required for the multiplicity (high dimensionality) of the energy release process, and a strong κ firmly establishes their interactions. Therefore, it is reasonable that the power-law fluctuation is prominent in the situation. However, certain results cannot be explained directly by the occurrence conditions of SOC. As shown in Figs. 5(a) and 5(b), the power-law behavior is prominent when $j_e = 1$ rather than when $j_e = 0$. It is a wonder that the onset of the power-law behavior is determined by the threshold of the solitary mode $j_e = 1$ rather than that of the external cavity modes $j_e = 0$, although the power-law behaviors depend strongly on the external feedback light. In future works, more efforts should be undertaken to explain the optimum value of the feedback strength, $\kappa/\kappa_{max} \simeq 0.6$, to obtain remarkable power-law fluctuations as shown in Fig. 5(c).

At a glance, the aforementioned conditions, particularly the requirement of the injection current tuning, appear to deviate from the concept of "self-organized" criticality. This is because parameters governing the conditions exist clearly in laser systems, whereas they are presumed implicitly in conventional SOC systems. For instance, forest fires or earthquakes, known as typical examples of SOC systems, seem to spontaneously organize a critical state without any fine tuning of parameters. The models of those phenomena have no explicit parameters for controlling energy injection rates as they introduce an infinite timescale separation a priori. This separation is attributed to the fact that the injection rates, such as tree growth and stress loading on a fault by the motion of the tectonic plates, are extremely slow compared to the energy release by fire spread in a forest and fault slip, respectively. The influence of the timescale separation on the criticality was discussed by Vespignani and coworkers, introducing a nonvanishing driving rate into the sandpile system, which is a traditional toy model of SOC [38]. By contrast, laser systems innately contain a parameter for naturally controlling the driving rate as the injection current. Hence, the laser with delayed feedback is an extraordinary example of SOC and can be a useful instance of embodying the effect of timescale separation on criticality.

Resonance often plays a key role in irregular laser oscillations, but the resonance is not expected to contribute to the power-law behavior in the present condition. The resonance considered here results from the interaction between the solitary mode, which is the intrinsic oscillation mode of the semiconductor lasers, and the optical feedback with the time delay τ. It is well known that the frequency of this solitary mode is described by $f_r = 1/(2\pi)\sqrt{(j-1)/(\tau_s\tau_p)(1+G_N N_0\tau_p)}$ [19], but the frequency is zero under the threshold condition ($j = 1$). Thus, the resonance with the solitary mode cannot occur for the threshold condition considered in the present paper [39]. The absence of the frequency is also consistent with

the power-law decay of the waiting time distribution at the threshold current depicted in Fig. 3, where the decay indicates that the characteristic timescale of the bursts is absent.

Next, we mention the discordance between the experimental and numerical results. The width of the power-law regime and the characteristic exponent obtained in our experiments vary slightly from the simulation results. The power-law regime obtained in the experiments is limited to one order of magnitude [from $I = 0.01$ to 0.1 in Fig. 8(a)] unlike the numerical results (Fig. 2). The lower bound would result from the noise of the measurement, whose size can be measured as the distribution in the nonoscillatory condition depicted by orange diamonds in Fig. 8(a). This noise region is almost consistent with the lower bound of the power-law regime of the experiments. The dynamic range of the measurement equipment used in the experiments is also a reason for the lower bound. The large characteristic exponent $\beta \simeq 2$ in the experiment compared with that in the simulations may have originated from the gain saturation of the laser and incomplete tuning of the pump current to the threshold value. The saturation effect reduces the cutoff of the intensity distributions (see Appendix B). The combination of the saturation effect and the excess pump current due to the incomplete tuning causes a partial increase in the gradient of the intensity distribution to 1.8 (Fig. 11).

Here, we indicate that the burst behavior is different from previously reported dynamical behaviors such as chaotic oscillations, RPPs, and LFFs. The pulses that construct the bursts may appear to be similar to RPPs, but, unlike RPPs, periodicity of the pulses is absent [19,25]. Even though the regular dropouts peculiar to LFFs are not observed in the burst behavior [19,24,27,28], LFFs may be associated with the power-law behaviors. This is because the condition for the emergence of the power-law bursts is close to that for LFFs except for the delay time. According to our investigation, depending on the feedback strength, regular drops can be observed when $\tau_D \lesssim 0.05$ ns, and a longer delay time causes the time series to be irregular. Future studies would elucidate the connection between the present power-law bursts and LFFs.

Finally, we discuss another factor that enhances the power-law behavior and its relationship with SOC. Even under the threshold condition with a sufficiently strong and long feedback, the intensity distribution still exhibits a sharp cutoff that restricts larger events, as shown in Fig. 2. According to the mean-field theory of SOC, dissipation in bulk and boundary regions of a system is essential for the criticality of SOC [38,40]. As semiconductor laser systems have no boundaries, here, we focus on the bulk dissipation, i.e., intrinsic dissipation. The intrinsic dissipation of semiconductor laser system is the spontaneous annihilation of carriers, whose timescale is determined by the carrier lifetime τ_s. Although the lifetime is a specific constant of the laser, it enables a change in the value in the numerical simulations. Figure 9 illustrates the intensity distribution obtained through simulations with different carrier lifetimes $\tilde{\tau}_s = \tau_s/64$, $\tau_s/8$, τ_s, $8\tau_s$, and $64\tau_s$. As shown in the figure, a long carrier lifetime (i.e., small intrinsic dissipation) makes the cutoff of the distributions large and the distributions approach a pure power-law distribution. This is consistent with the conclusion of the mean-field theory of SOC [38,40].

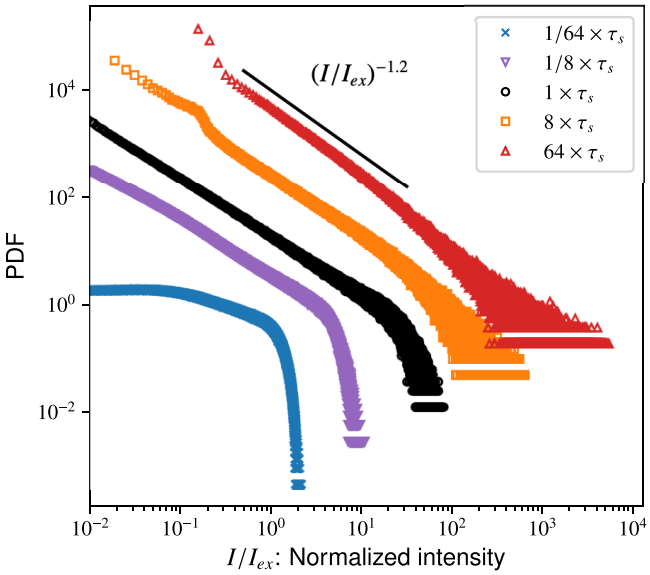

FIG. 9. The intensity distribution with the different carrier lifetime $\tilde{\tau}_s$. The distributions become to loose their cutoff and exhibit a simple power-law decay as $\tilde{\tau}_s$ is longer.

When carrier lifetime is too long, however, the criticality characterized using the cutoff of the power-law distribution breaks. We show the maximum intensity values as a function of $\tilde{\tau}_s$ normalized by the delay time τ in Fig. 10. The maximum intensity increases almost linearly. However, this trend breaks down in a regime where $\tilde{\tau}$ is close to τ. The delay time must be sufficiently longer than the carrier lifetime to achieve the power-law behavior. Therefore, the criticality of this delay system is expected to be attained at the limits where $\tilde{\tau}_s \to \infty$, $\tau \to \infty$, where $\tilde{\tau}_s < \tau$.

Nonequilibrium critical phenomena, namely SOC mentioned here, are closely related to nonequilibrium phase

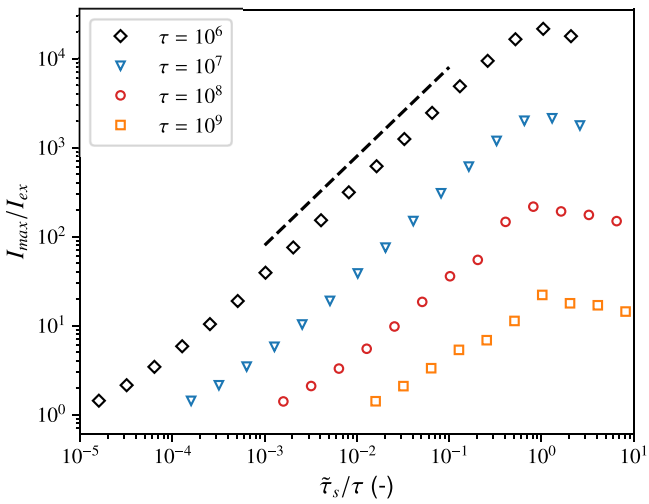

FIG. 10. Relative maximum intensity as a function of carrier lifetime $\tilde{\tau}_s$, where the lifetime is normalized by delay time τ. The maximum intensity increases with increasing $\tilde{\tau}_s$, but the trend disappears as $\tilde{\tau}_s$ exceeds τ, where the dashed line represents the linear relation, $I_{\max}/I_{\mathrm{ex}} \sim \tilde{\tau}_s/\tau$.

transitions, particularly the absorbing-state phase transition [41–43]. In fact, absorbing-state phase transition has been observed in a semiconductor laser with delayed feedback similar to that in the present study [44]. It is also noteworthy that the dynamical systems with time delays can produce SOC-like behaviors, in contrast to the fact that the conventional models that reproduce SOC and absorbing-state phase transitions generally consist of cellular automata [9,14,15,18]. The manner in which the delay system produces the power-law behaviors can be observed as a trajectory in the phase space as depicted in Fig. 4. Since most of the discussion on the relationship between the present results and SOC is conjectural, the detailed mechanism that produces the SOC features in delay systems should be elucidated in future studies. It might enable the understanding of nonequilibrium critical phenomena and phase transitions from the aspect of dynamical systems in the presence of delayed feedback.

V. CONCLUSIONS

In the present simulations and experiments, we demonstrated that the semiconductor lasers with a sufficiently strong and long delayed feedback at the critical point (lasing threshold) can cause the intermittent intensity fluctuation characterized by power-law distributions typical in nonequilibrium critical phenomena. The results of the numerical simulations of the Lang-Kobayashi model show that the laser intensity exhibits irregular bursts consisting of spike-like pulsation. As a result, certain peak values of the bursts attain several tens of times the intensity of the maximum gain mode. This is quantitatively different from other currently reported behaviors such as low-frequency fluctuations, regular pulse packages, or chaotic oscillations. Similar behaviors were experimentally measured in a semiconductor laser with delayed feedback. The intensity bursts are most remarkable when the coupling of the feedback is moderately strong (60% of the maximum feedback strength), the delay time is sufficiently long ($\tau > 1$ ns), and the pump current is just on the threshold value of the solitary mode. The noteworthy feature is that the intensity and waiting time of the bursts follow power-law distributions with exponents of approximately 1 and 2/3, respectively. Additional simulations indicate another non-trivial condition for the power-law behavior; The behavior is more remarkable when the carrier lifetime of the laser increases and the lifetime is shorter than the delay time. The statistical feature and the condition of the intermittent laser oscillation are analogous to self-organized criticality.

ACKNOWLEDGMENTS

S.S. thanks Dr. Kenichi Arai (NTT Communication Science Laboratories) for his support for the laser experiment. This work was partly supported by JSPS KAKENHI (Grants No. 20K03783, No. 20H04255, and No. 22H05198) and JST PRESTO (Grant No. JPMJPR19M4).

APPENDIX A: CHARACTERISTIC VALUES OF EXTERNAL CAVITY MODES

To investigate the intensity dynamics of the lasers, in this paper, we employed certain quantities that represent external cavity modes of semiconductor lasers described by the Lang-Kobayashi equations; the oscillation intensity of maximum gain mode I_{ex}, threshold current of the external cavity modes J_{ex}, and maximum strength of the delayed feedback κ_{max}. Although these are described in commonly available textbooks [19], we introduce these quantities in this Appendix for the reader's convenience.

The intensity generated from the maximum gain mode can be estimated by considering the stationary state of the Lang-Kobayashi equation $d\hat{E}/dt = dN/dt = 0$. The stationary carrier density N_s when $d\hat{E}/dt = 0$ is obtained from Eq. (2):

$$N_s = N_{th} - \frac{2\kappa}{G_N}\cos\omega_s\tau \tag{A1}$$

where $N_{th} = N_0 + 1/(\tau_p G_0)$, and ω_s is a stationary angular frequency. Substituting the carrier density into Eq. (3), we can obtain the stationary intensity of external cavity modes described by the square of $\hat{E}$,

$$I_s = \frac{\tau_p}{G_N\tau_s}\frac{(j-1)N_{th}G_N + 2\kappa\cos\omega_s\tau}{1 - 2\tau_p\kappa\cos\omega_s\tau}, \tag{A2}$$

where j is the normalized pump current defined by $j = J/J_{th}$, and $J_{th} = N_{th}/\tau_s$. Because I_s is determined by the angular frequency of a mode ω_s, it is maximized when $\cos\omega_s\tau = 1$. Hence, the intensity of the maximum gain mode that we used to normalize the intensity of oscillation in this study can be represented by

$$I_{ex} = \frac{1}{G_N}\frac{\tau_p}{\tau_s}\frac{(j-1)N_{th}G_N + 2\kappa}{1 - 2\tau_p\kappa}. \tag{A3}$$

The condition $I_{ex} = 0$ means that at least one external cavity mode begins to oscillate. Thus, the external cavity mode can activate at the normalized pump current $j = 1 - 2\kappa/(N_{th}G_N)$. Then the threshold pump current is represented by

$$J_{ex} = J_{th}\left(1 - \frac{2\kappa}{N_{th}G_N}\right). \tag{A4}$$

From the denominator of Eq. (A3), we can recognize that the stationary intensity is finite unless $2\tau_p\kappa \geqslant 1$. Therefore, the maximum feedback strength that we can set is determined by

$$\kappa_{max} = (2\tau_p)^{-1}. \tag{A5}$$

These estimations are good approximations as long as the number of external cavity modes is sufficiently large.

APPENDIX B: SATURATION EFFECT OF GAIN

To extract the essence of power-law behaviors in semiconductor lasers with delayed feedback, we omitted the effect of gain saturation of the laser in the simulations of this study. However, the saturation effect is essential for comparing the present simulations with the experiments. Here, we show the influence of the gain saturation upon the intensity distributions by performing simulations of the Lang–Kobayashi model with the nonvanishing gain saturation parameter ϵ shown in Eq. (4). For the simulations, we applied some values of the saturation parameter in the range from $\epsilon = 10^{-23}\,\mathrm{m}^3$ to $5.0 \times 10^{-23}\,\mathrm{m}^3$,

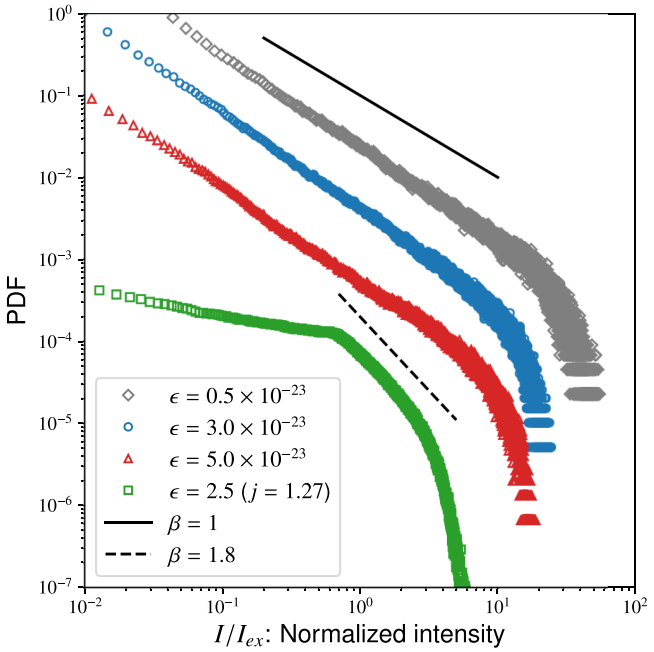

FIG. 11. PDF of oscillation intensity for different gain saturation parameters ϵ with the threshold injection current $j = 1$, where the distribution depicted by green squares is for $\epsilon = 2.5 \times 10^{-23}\,\mathrm{m}^3$ and $j = 1.2652$. For visibility, power-law curves with exponents $\beta = 1$ and 1.8 are shown by solid and dashed lines, respectively.

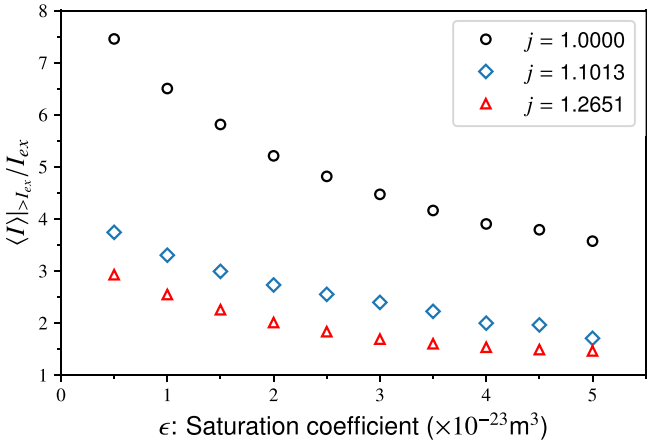

FIG. 12. The mean exceedance of the intensity for different injection currents j as a function of the saturation parameter ϵ, where the exceedance is normalized by I_{ex}.

where the range includes the value of actual lasers used in ordinary experiments [45,46].

The intensity distributions with three gain saturation parameters are shown in Fig. 11, where the gray diamonds, blue circles, and red triangles correspond to $\epsilon = 10^{-23}$, 3.0×10^{-23}, and $10^{-23}\,\mathrm{m}^3$, respectively, and the pump current of the three distribution is set as the threshold value of the solitary mode ($j = 1$). As is evident from the figure, the results of $\epsilon = 10^{-23}$ and $3.0 \times 10^{-23}\,\mathrm{m}^3$ exhibit power-law distributions with $\beta \simeq 1$ that are identical to those obtained by the simulations with $\epsilon = 0$. The larger saturation parameter ($\epsilon = 5.0 \times 10^{-23}\,\mathrm{m}^3$) affects its distribution slightly.

A more significant influence of the gain saturation is a decrease in the cutoff of the distributions with an increase in ϵ. This trend can be confirmed more clearly in Fig. 12, where the mean exceedance above I_{ex} is plotted as a function of ϵ. The figure indicates that the maximum intensity caused by oscillation bursts decreases monotonically with ϵ regardless of j. Another notable result can be observed in the distribution as shown by green squares in Fig. 11. Here, its saturation parameter, $\epsilon = 2.5 \times 10^{-23}\,\mathrm{m}^3$, is comparable with that used for the present experiments described in Sec. III, and the pump current is slightly larger than the solitary mode threshold, $j = 1.2652$. The distribution indicates that a synergy between the gain saturation and the excess of the current disrupts a wide range of power-law regimes, and the gradient of the power-law regime of the distribution increases more than $\beta = 1.8$. This implies that power-law statistics different from that obtained in the simulations can be observed in the experimental measurements because it is hard to tune the injection current just to the threshold value of the solitary mode and the saturation effect is consistently present in actual lasers.

The decrease in the cutoff of the intensity distribution due to the gain-saturation effect can be explained in terms of the SOC framework. Gain saturation is considered to be a type of dissipation in laser systems. As discussed through mean-field theory [38,40], intrinsic dissipation and/or the finite-size effect weaken the criticality (see also the dependence of the carrier lifetime in Sec. IV). Thus, the shortening the width of the scaling region by introducing the gain saturation can be understood as the influence of such effects.

[1] V. DeGiorgio and M. O. Scully, Analogy between the laser threshold region and a second-order phase transition, Phys. Rev. A **2**, 1170 (1970).

[2] R. Graham and H. Haken, Laserlight—First example of a second-order phase transition far away from thermal equilibrium, Z. Phys. **237**, 31 (1970).

[3] P. R. Rice and H. J. Carmichael, Photon statistics of a cavity-QED laser: A comment on the laser–phase-transition analogy, Phys. Rev. A **50**, 4318 (1994).

[4] W.-C. Kuo, Y.-H. Wu, Y.-C. Li, and T.-C. Yen, Criticalities and phase transitions in the polarization switching of vertical-cavity surface-emitting lasers, IEEE Photonics Technol. Lett. **24**, 2262 (2012).

[5] S. Basak, A. Blanco, and C. López, Large fluctuations at the lasing threshold of solid- and liquid-state dye lasers, Sci. Rep. **6**, 32134 (2016).

[6] T. Wang, H. Vergnet, G. P. Puccioni, and G. L. Lippi, Dynamics at threshold in mesoscale lasers, Phys. Rev. A **96**, 013803 (2017).

[7] T. Wang, G. P. Puccioni, and G. L. Lippi, Photon bursts at lasing onset and modelling issues in micro-vcsels, J. Mod. Opt. **67**, 55 (2020).

[8] D. Sornette, *Critical Phenomena in Natural Sciences: Chaos, Fractals, Selforganization and Disorder: Concepts and Tools* (Springer Science & Business Media, New York, 2006).

[9] M. Aschwanden, *Self-Organized Criticality in Astrophysics: The Statistics of Nonlinear Processes in the Universe* (Springer, New York, 2011).

[10] F. Omori, On the after-shocks of earthquakes, J. Coll. Sci., Imp. Univ., Japan **7**, 111 (1895).

[11] T. Utsu, Aftershocks and earthquake statistics (i) : Some parameters which characterize an aftershock sequence and their interrelations, J. Faculty Sci., Hokkaido University, Ser. VII (Geophys.) **3**, 129 (1970).

[12] M. C. Miguel, A. Vespignani, S. Zapperi, J. Weiss, and J.-R. Grasso, Intermittent dislocation flow in viscoplastic deformation, Nature (London) **410**, 667 (2001).

[13] T. Niiyama and T. Shimokawa, Atomistic mechanisms of intermittent plasticity in metals: Dislocation avalanches and defect cluster pinning, Phys. Rev. E **91**, 022401 (2015).

[14] P. Bak, C. Tang, and K. Wiesenfeld, Self-Organized Criticality: An Explanation of the 1/f Noise, Phys. Rev. Lett. **59**, 381 (1987).

[15] P. Bak, C. Tang, and K. Wiesenfeld, Self-organized criticality, Phys. Rev. A **38**, 364 (1988).

[16] G. Durin and S. Zapperi, Scaling Exponents for Barkhausen Avalanches in Polycrystalline and Amorphous Ferromagnets, Phys. Rev. Lett. **84**, 4705 (2000).

[17] S. Field, J. Witt, F. Nori, and X. Ling, Superconducting Vortex Avalanches, Phys. Rev. Lett. **74**, 1206 (1995).

[18] H. J. Jensen, *Self-Organized Criticality: Emergent Complex Behavior in Physical and Biological Systems* (Cambridge Lecture Notes in Physics) (Cambridge University Press, Cambridge, 1998).

[19] A. Uchida, *Optical Communication with Chaotic Lasers: Applications of Nonlinear Dynamics and Synchronization* (John Wiley & Sons, Hoboken, NJ, 2012).

[20] K. Ikeda and K. Matsumoto, High-dimensional chaotic behavior in systems with time-delayed feedback, Physica D **29**, 223 (1987).

[21] F. T. Arecchi, G. Giacomelli, A. Lapucci, and R. Meucci, Two-dimensional representation of a delayed dynamical system, Phys. Rev. A **45**, R4225 (1992).

[22] G. Giacomelli and A. Politi, Relationship between Delayed and Spatially Extended Dynamical Systems, Phys. Rev. Lett. **76**, 2686 (1996).

[23] T. Erneux, J. Javaloyes, M. Wolfrum, and S. Yanchuk, Introduction to focus issue: Time-delay dynamics, Chaos **27**, 114201 (2017).

[24] J. Ohtsubo, *Semiconductor Lasers: Stability, Instability and Chaos*, Vol. 111 (Springer, New York, 2012).

[25] T. Heil, I. Fischer, W. Elsäßer, and A. Gavrielides, Dynamics of Semiconductor Lasers Subject to Delayed Optical Feedback: The Short Cavity Regime, Phys. Rev. Lett. **87**, 243901 (2001).

[26] K. Ikeda, H. Daido, and O. Akimoto, Optical Turbulence: Chaotic Behavior of Transmitted Light from a Ring Cavity, Phys. Rev. Lett. **45**, 709 (1980).

[27] I. Fischer, G. H. M. van Tartwijk, A. M. Levine, W. Elsässer, E. Göbel, and D. Lenstra, Fast Pulsing and Chaotic Itinerancy with a Drift in the Coherence Collapse of Semiconductor Lasers, Phys. Rev. Lett. **76**, 220 (1996).

[28] T. Heil, I. Fischer, and W. Elsäßer, Coexistence of low-frequency fluctuations and stable emission on a single high-gain mode in semiconductor lasers with external optical feedback, Phys. Rev. A **58**, R2672 (1998).

[29] J. A. Reinoso, J. Zamora-Munt, and C. Masoller, Extreme intensity pulses in a semiconductor laser with a short external cavity, Phys. Rev. E **87**, 062913 (2013).

[30] A. K. D. Bosco, D. Wolfersberger, and M. Sciamanna, Extreme events in time-delayed nonlinear optics, Opt. Lett. **38**, 703 (2013).

[31] D. Choi, M. J. Wishon, J. Barnoud, C. Y. Chang, Y. Bouazizi, A. Locquet, and D. S. Citrin, Low-frequency fluctuations in an external-cavity laser leading to extreme events, Phys. Rev. E **93**, 042216 (2016).

[32] A. K. D. Bosco, N. Sato, Y. Terashima, S. Ohara, A. Uchida, T. Harayama, and M. Inubushi, Random number generation from intermittent optical chaos, IEEE J. Sel. Top. Quantum Electron. **23**, 1 (2017).

[33] W. A. S. Barbosa, E. J. Rosero, J. R. Tredicce, and J. R. Rios Leite, Statistics of chaos in a bursting laser, Phys. Rev. A **99**, 053828 (2019).

[34] L. Appeltant, M. C. Soriano, G. Van der Sande, J. Danckaert, S. Massar, J. Dambre, B. Schrauwen, C. R. Mirasso, and I. Fischer, Information processing using a single dynamical node as complex system, Nat. Commun. **2**, 468 (2011).

[35] L. Larger, A. Baylón-Fuentes, R. Martinenghi, V. S. Udaltsov, Y. K. Chembo, and M. Jacquot, High-Speed Photonic Reservoir Computing Using a Time-Delay-Based Architecture: Million Words per Second Classification, Phys. Rev. X **7**, 011015 (2017).

[36] R. Lang and K. Kobayashi, External optical feedback effects on semiconductor injection laser properties, IEEE J. Quantum Electron. **16**, 347 (1980).

[37] B. Gutenberg and C. F. Richter, Earthquake magnitude, intensity, energy, and acceleration, Bull. Seismol. Soc. Am. **46**, 105 (1956).

[38] A. Vespignani and S. Zapperi, How self-organized criticality works: A unified mean-field picture, Phys. Rev. E **57**, 6345 (1998).

[39] Whereas there are some external cavity modes, it is not easy to determine the frequencies of these modes even in a short and weak feedback condition (see the reference), so their interactions are the future work. Y. Liu, N. Kikuchi, and J. Ohtsubo, Controlling dynamical behavior of a semiconductor laser with external optical feedback, Phys. Rev. E **51**, R2697 (1995).

[40] A. Vespignani and S. Zapperi, Order Parameter and Scaling Fields in Self-Organized Criticality, Phys. Rev. Lett. **78**, 4793 (1997).

[41] M. A. Muñoz, R. Dickman, A. Vespignani, and S. Zapperi, Avalanche and spreading exponents in systems with absorbing states, Phys. Rev. E **59**, 6175 (1999).

[42] A. Vespignani, R. Dickman, M. A. Muñoz, and S. Zapperi, Absorbing-state phase transitions in fixed-energy sandpiles, Phys. Rev. E **62**, 4564 (2000).

[43] M. Henkel, H. Hinrichsen, and S. Lübeck, *Non-Equilibrium Phase Transitions: Vol. 1: Absorbing Phase Transitions* (Springer Science & Business Media, 2008).

[44] M. Faggian, F. Ginelli, F. Marino, and G. Giacomelli, Evidence of a Critical Phase Transition in Purely Temporal Dynamics

with Long-Delayed Feedback, Phys. Rev. Lett. **120**, 173901 (2018).

[45] T. Harayama, S. Sunada, K. Yoshimura, P. Davis, K. Tsuzuki, and A. Uchida, Fast nondeterministic random-bit generation using on-chip chaos lasers, Phys. Rev. A **83**, 031803(R) (2011).

[46] T. Mikami, K. Kanno, K. Aoyama, A. Uchida, T. Ikeguchi, T. Harayama, S. Sunada, K.-i. Arai, K. Yoshimura, and P. Davis, Estimation of entropy rate in a fast physical random-bit generator using a chaotic semiconductor laser with intrinsic noise, Phys. Rev. E **85**, 016211 (2012).